

Investigation of Volume Phase Transition from the Different Properties of Particles

Yong Sun*

November 28, 2017

Abstract

In this work, three different particle sizes: the static radius R_s , hydrodynamic radius R_h and apparent hydrodynamic radius $R_{h,app}$ obtained using the light scattering technique, are investigated for dilute poly-disperse homogenous spherical particles with a simple assumption that the hydrodynamic radius is in proportion to the static radius, when the Rayleigh-Gans-Debye approximation is valid. The results show that the expected values of the normalized time auto-correlation function of the scattered light intensity $g^{(2)}(\tau)$ calculated based on the static particle size information are consistent with the experimental data. The volume phase transition is thus investigated using the equilibrium swelling ratios of static radii and apparent hydrodynamic radii respectively. The changes of the static particle size information and apparent hydrodynamic radius as a function of temperature T show the effects of the volume phase transition on optical properties and the total influences of the volume phase transition on the optical, hydrodynamic characteristics and size distribution of particles, respectively. The effects of cross-linker on the volume phase transition are also discussed.

1 INTRODUCTION

A great deal of information about particles in dispersion can be measured using the light scattering technique. One of the main applications of the light scattering technique is that measures the particle sizes. The static light scattering technique (SLS) measures the size information from the optical characteristics and the dynamic light scattering technique (DLS) obtains the size information from both the optical and hydrodynamic features of particles.

For a long time, the standard method of cumulants [1–4] has been used to measure the apparent hydrodynamic radius $R_{h,app}$ of particles from the normalized time auto-correlation function of the scattered light intensity $g^{(2)}(\tau)$ with the assistance of the Einstein-Stokes relation, where τ is the delay time. The equilibrium swelling ratios [5, 6] of $R_{h,app}^T$ at temperature T over $R_{h,app}^{T_0}$ at temperature T_0 are used to show the volume phase transition. Due to the fact that $R_{h,app}^T$ is determined by the optical,

*Email: ysun2002h@yahoo.com.cn

hydrodynamic characteristics and size distribution of particles and scattering vector [7], the equilibrium swelling ratios show the total changes of the optical, hydrodynamic characteristics and size distribution of particles as a function of temperature T . The treatment of SLS is simplified to the Zimm plot, Berry plot or Guinier plot etc. to obtain the root mean-square radius of gyration $\langle R_g^2 \rangle^{1/2}$ and the molar mass of particles provided that the particle sizes are small [4, 8]. In order to obtain more information about the particles, people have explored the relationships among the physical quantities measured using the SLS and DLS techniques respectively. The measurements of the dimensionless shape parameter $\rho = \langle R_g^2 \rangle^{1/2} / R_{h,app}$ [8–12] have been extensively used to infer the structures of particles for a long time. In this judgement, it has an assumption that the particle sizes measured from SLS and DLS are the same. However, the particle sizes measured from SLS and DLS are different quantities [7]. Exactly using the light scattering technique, three different sizes can be measured for dilute poly-disperse homogenous spherical particles in dispersion: one is a static radius R_s measured from the optical characteristics; the second is a hydrodynamic radius R_h obtained from the hydrodynamic features and the third is an apparent hydrodynamic radius $R_{h,app}$ determined by the optical, hydrodynamic characteristics and size distribution of particles and scattering angle.

In this work, the three different particle sizes will be investigated using Poly(*N*-isopropylacrylamide)(PNIPAM) microgel samples with a simple assumption that hydrodynamic radius R_h is in proportion to the static radius R_s . The results show that the expected values of $g^{(2)}(\tau)$ calculated based on the particle size information obtained using the static light technique are consistent with the experimental data, the difference between the mean static radius and apparent hydrodynamic radius is large and the difference between the mean hydrodynamic radius and apparent hydrodynamic radius is influenced by the particle size distribution. The volume phase transition is thus investigated using the equilibrium swelling ratios of static radii and apparent hydrodynamic radii respectively. The changes of the static particle size information and apparent hydrodynamic radius as a function of temperature T show the effects of the volume phase transition on optical properties and the total influences of the volume phase transition on the optical, hydrodynamic characteristics and size distribution of particles, respectively. The effects of cross-linker on the volume phase transition are also discussed.

2 THEORY

For dilute poly-disperse homogeneous spherical particles in dispersion where the Rayleigh-Gans-Debye (RGD) approximation is valid, the normalized time auto-correlation function of the electric field of the scattered light $g^{(1)}(\tau)$ is given by

$$g^{(1)}(\tau) = \frac{\int_0^\infty R_s^6 P(q, R_s) G(R_s) \exp(-q^2 D\tau) dR_s}{\int_0^\infty R_s^6 P(q, R_s) G(R_s) dR_s}, \quad (1)$$

where R_s is the static radius, D is the diffusion coefficient, $q = \frac{4\pi}{\lambda} n_s \sin \frac{\theta}{2}$ is the scattering vector, λ is the wavelength of the incident light in vacuo, n_s is the solvent refractive index, θ is the scattering angle, $G(R_s)$ is the number distribution of particle sizes and the form factor $P(q, R_s)$ is

$$P(q, R_s) = \frac{9}{q^6 R_s^6} (\sin(qR_s) - qR_s \cos(qR_s))^2. \quad (2)$$

In this work, the number distribution is chosen as a Gaussian distribution

$$G(R_s; \langle R_s \rangle, \sigma) = \frac{1}{\sigma \sqrt{2\pi}} \exp \left(-\frac{1}{2} \left(\frac{R_s - \langle R_s \rangle}{\sigma} \right)^2 \right), \quad (3)$$

where $\langle R_s \rangle$ is the mean static radius and σ is the standard deviation related to the mean static radius.

From the Einstein-Stokes relation

$$D = \frac{k_B T}{6\pi\eta_0 R_h}, \quad (4)$$

where η_0 , k_B and T are the viscosity of the solvent, Boltzmann's constant and absolute temperature respectively, the hydrodynamic radius R_h can be obtained.

For simplicity, the relationship between the static and hydrodynamic radii is assumed to be

$$R_h = aR_s, \quad (5)$$

where a is a constant. From the Siegert relation between $g^{(2)}(\tau)$ and $g^{(1)}(\tau)$ [13]

$$g^{(2)}(\tau) = 1 + \beta \left(g^{(1)} \right)^2, \quad (6)$$

the function between the static and dynamic light scattering is built and the values of $g^{(2)}(\tau)$ can be expected based on the size information obtained using the SLS technique.

If the first cumulant is used to measure the apparent hydrodynamic radius $R_{h,app}$, the constant a can be determined approximately using

$$a = \frac{R_{h,app} \int_0^\infty R_s^6 P(q, R_s) G(R_s) dR_s}{\int_0^\infty R_s^7 P(q, R_s) G(R_s) dR_s}. \quad (7)$$

3 EXPERIMENT

The SLS and DLS data were measured using the instrument built by ALV-Laser Vertriebsgesellschaft m.b.H (Langen, Germany). It utilizes an ALV-5000 Multiple Tau Digital Correlator and a JDS Uniphase 1145P He-Ne laser to provide a 23 mW vertically polarized laser at wavelength of 632.8 nm.

The PNIPAM microgel samples used in this work have been detailed before [7]. The four PNIPAM microgel samples PNIPAM-0, PNIPAM-1, PNIPAM-2 and PNIPAM-5 were named according to the molar ratios n_B/n_N of cross-linker N, N' -methylenebisacrylamide over N -isopropylacrylamide.

Temperature (°C)	$\langle R_s \rangle$ (nm)	σ (nm)	χ^2
25	277.7±0.5	23.1±0.9	1.84
27	267.1±0.5	23.1±0.8	2.50
29	254.3±0.1	21.5±0.3	2.15
31	224.8±0.9	30.6±0.9	3.31
33	119.9±0.9	19.8±0.6	3.16
36	110.4±0.9	17.3±0.7	4.19
40	111.7±0.9	14.8±0.8	2.73

Table 1: The particle sizes obtained from SLS for PNIPAM-1 at different temperatures.

Scattering Angle	$R_{h,app}$ (nm)	a
30°	329.±4.	1.19
35°	331.1±0.7	1.21
40°	329.6±0.9	1.21
45°	329.8±0.5	1.22
50°	329.±1.	1.22
55°	326.4±0.2	1.23
60°	327.±2.	1.25
65°	323.±2.	1.26

Table 2: Values of the apparent hydrodynamic radius and constant a for PNIPAM-1 at different scattering angles and a temperature of 27 °C.

4 RESULTS AND DISCUSSION

The mean static radius $\langle R_s \rangle$ and standard deviation σ of the four PNIPAM microgel samples are measured from the SLS data [7]. For PNIPAM-1, the mean static radii $\langle R_s \rangle$, standard deviations σ and χ^2 obtained at different temperatures are listed in Table 1.

The values of the apparent hydrodynamic radius at different scattering angles were measured using the first cumulant analysis. In order to avoid the consideration for the large values of χ^2 , all the fit results obtained using the first cumulant analysis are chosen under this condition $\chi^2 \leq 2$. For PNIPAM-1 at a temperature of 27 °C, the values of the apparent dynamic radius at different scattering angles are listed in Table 2. The ratios of the hydrodynamic radius over the static radius calculated using Eq. 7 at different scattering angles are also listed in Table 2.

From the results shown in Table 2, the values of a at different scattering angles are almost equal. If the value of constant a was set to 1.21, the expected values of $g^{(2)}(\tau)$ calculated based on the mean static radius $\langle R_s \rangle$ and standard deviation σ using Eqs. 1, 5 and 6 were compared with the experimental data measured at scattering angles 30°, 45° and 65°, respectively. The results are shown in Fig. 1. The expected values are consistent with the experimental data. With the constant a : 1.21, the mean hydrody-

Scattering Angle	$R_{h,app}$ (nm)	a
30°	212.1±0.6	1.55
35°	208.3±0.2	1.53
40°	208.7±0.6	1.54
45°	207.3±0.3	1.53
50°	206.7±0.4	1.53
55°	206.±1.	1.53
60°	205.±1.	1.53
65°	204.9±0.6	1.54
70°	205.±1.	1.55
75°	205.±1.	1.56
80°	205.±1.	1.56
85°	205.±1.	1.57
90°	203.2±0.7	1.57
95°	204.±1.	1.58

Table 3: Values of the apparent hydrodynamic radius and constant a for PNIPAM-1 at different scattering angles and a temperature of 33 °C.

namic radius 323.2 ± 0.6 nm can be obtained and this value only has little different from the values of the apparent hydrodynamic radius measured using the first cumulant at different scattering angles.

From the results shown in Table 1, at a temperature of 33 °C, the particle size distribution of PNIPAM-1 is wide. Its corresponding values of the apparent hydrodynamic radius are listed in Table 3. The ratios of the hydrodynamic radius over the static radius calculated using Eq. 7 are also listed in Table 3. The values of a at different scattering angles are almost equal. If the value of constant a was set to 1.55, the expected values of $g^{(2)}(\tau)$ calculated based on $\langle R_s \rangle$ and σ using Eqs. 1, 5 and 6 were compared with the experimental data measured at scattering angles 30°, 60° and 90°, respectively. The results are shown in Fig. 2. The expected values are consistent with the experimental data. With the constant a : 1.55, the mean hydrodynamic radius $186.\pm1.$ nm is obtained and the difference between the mean hydrodynamic radius and apparent hydrodynamic radius is large.

From the results above, three different particle sizes can be measured using the light scattering technique. In general, the values of the constant a and apparent hydrodynamic radius $R_{h,app}$ vary with the scattering angle. In order to compare the three different particle sizes conveniently, all the mean hydrodynamic and apparent hydrodynamic radii were obtained at a scattering angle of 30°. All the three particle sizes measured at different temperatures for PNIPAM-1 are shown in Fig. 3. The figure shows that the difference between the mean static radius and apparent hydrodynamic radius is large and the difference between the mean hydrodynamic radius and apparent hydrodynamic

radius is influenced by the particle size distribution. The figure also shows that when the temperature nears the phase transition temperature, all the radii have a sharp change and the volumes of PNIPAM-1 collapse.

The three different particle sizes represent the different characteristics of particles. When temperature changes from 25 °C to 40 °C, the property of the PNIPAM microgel samples changes from being hydrophilic to hydrophobic. The volumes of PNIPAM microgel particles collapse. It is possible that this change makes the different influences on the optical and hydrodynamic characteristics of particles. In order to show the effects of the volume phase transition, the ratios $R_{h,app}^T / \langle R_s^T \rangle$ and $\langle R_h^T \rangle / \langle R_s^T \rangle$ as a function of temperature T are shown in Figs. 4a and 4b, respectively.

Figure 4 shows that the effects of the phase volume transition on the optical and hydrodynamic characteristics of particles are different. The differences are also influenced by the *N,N'*-methylenebisacrylamide content. When the temperature nears the phase transition temperature, the values of the ratios $R_{h,app}^T / \langle R_s^T \rangle$ and $\langle R_h^T \rangle / \langle R_s^T \rangle$ become larger and peaks emerge. Figure 4a shows that the lower the crosslinker content, the higher the peak. Figure 4b shows that the effects of the crosslinker content is not so striking. From the static particle size distributions of the four PNIPAM microgel samples, the particle size distributions are narrow both below and above the phase transition and are wide near the phase transition. The particle size distribution is also becoming narrow when the *N,N'*-methylenebisacrylamide content is increased in the vicinity of the phase transition temperature. From the theoretical analysis of cumulants, the apparent hydrodynamic radius is obtained from averaging the term $\exp(-q^2 D\tau)$ in static particle size distribution $G(R_s)$ with the weight $R_s^6 P(q, R_s)$, where $\exp(-q^2 D\tau)$ represents the hydrodynamic features of particles. For the mono-disperse particle systems, since the effects of scattered intensity are cancelled, the apparent hydrodynamic radius is equal to the hydrodynamic radius. For poly-disperse particle systems, the apparent hydrodynamic radius is different from the mean hydrodynamic radius and is also determined by the particle size distribution [7]. Comparing Figs. 4a with 4b, the difference between the apparent hydrodynamic radius and mean hydrodynamic radius is influenced obviously by the distribution width.

Since the PNIPAM microgels possess the temperature sensitivity in the temperature range 15 °C - 50 °C, a few authors [12, 13] used the equilibrium swelling ratios $R_{h,app}^T / R_{h,app}^{T_0}$ of the apparent hydrodynamic radius at temperature T over that at temperature T_0 to show the volume phase transition. For the four PNIPAM microgel samples, the volume phase transition in the temperature range 25 °C - 40 °C is shown in Fig. 5 using the equilibrium swelling ratios of the mean static radii and the apparent hydrodynamic radii, respectively. All radii are compared to that measured at a temperature of 40 °C. The ratios $\langle R_s^T \rangle / \langle R_s^{40^\circ C} \rangle$ and $R_{h,app}^T / R_{h,app}^{40^\circ C}$ are shown in Fig. 5a and 5b respectively. Figure 5a shows the volume phase transition is investigated using the optical properties and Figure. 5b shows the volume phase transition is investigated using the optical, hydrodynamic characteristics and size distribution of particles together.

From the material characteristics, the materials of PNIPAM possess the temperature

sensitivity. If adding the N, N' -methylenebisacrylamide, the temperature sensitivity of PNIPAM microgels is influenced by the content of the N, N' -methylenebisacrylamide which does not possess the temperature sensitivity. If the content of the N, N' -methylenebisacrylamide continues to increase, the temperature sensitivity of PNIPAM microgels is becoming weak. Figure 5 shows clearly the feature. The phase transition of PNIPAM microgels, indicated as the ratios $\langle R_s^T \rangle / \langle R_s^{40^\circ C} \rangle$ or $R_{h,app}^T / R_{h,app}^{40^\circ C}$ as a function of T , becomes less sharp and occurs in a broader T range as the N, N' -methylenebisacrylamide content is increased.

In general, from the SLS data the root mean-square radius of gyration $\langle R_g^2 \rangle^{1/2}$ is obtained provided that the particle sizes are small and from DLS data the hydrodynamic radius is got. The dimensionless shape parameter ρ , the ratio of $\langle R_g^2 \rangle^{1/2}$ to the hydrodynamic radius, has been extensively used to infer the structure of particles [8–10] and the change of ρ as a function of temperature T during the volume phase transition range has been explored by a few authors [11,12]. Because the static and hydrodynamic radii are different quantities and particles have a size distribution, $\langle R_g^2 \rangle^{1/2} / \langle R_s^T \rangle$ is determined not only by the structure of particles but also the particle size distribution and ρ includes not only the relationship between $\langle R_g^2 \rangle^{1/2}$ and $\langle R_s^T \rangle$ but also the function between $\langle R_s^T \rangle$ and $R_{h,app}^T$. Since the effects of the volume phase transition on the optical and hydrodynamic characteristics of particles are different, the dimensionless parameters $\langle R_g^2 \rangle^{1/2} / \langle R_s^T \rangle$ and ρ as a function of temperature T are shown in Figs. 6a and 6b, respectively. $\langle R_g^2 \rangle^{1/2}$ was obtained using the relationship between the $\langle R_g^2 \rangle^{1/2}$ and static size information [7]. As shown in Fig. 6a, the dimensionless parameter $\langle R_g^2 \rangle^{1/2} / \langle R_s^T \rangle$ is larger than 0.775 due to the effects of the particles size distribution. When the temperature nears the phase transition temperature, the values of the ratios $\langle R_g^2 \rangle^{1/2} / \langle R_s^T \rangle$ become larger and peaks emerge. Since the larger the value, the wider the particle size distribution, peaks show that the particle size distribution become wide when the temperature nears the volume phase transition temperature. ρ has a very interesting change as a function of temperature T as shown in Fig. 6b. When the temperature nears the phase transition temperature, the values of the ratios ρ become smaller and minimums emerge. Since the accurate relationship between the optical and hydrodynamic features of particles has not been understood, the meanings of ρ need to be discussed further.

5 CONCLUSION

Using the light scattering technique, three different particle sizes can be measured. The static radius represents the optical characteristics, the hydrodynamic radius shows the hydrodynamic features and the apparent hydrodynamic radius is determined by the optical, hydrodynamic characteristics and size distribution of particles and scattering angle. The difference between the mean static radius and apparent hydrodynamic radius is large and the difference between the mean hydrodynamic radius and apparent hydrodynamic radius is influenced by the particle size distribution. The changes of the static particle size information and apparent hydrodynamic radius as a function of tem-

perature T show the effects of the volume phase transition on optical properties and the total influences of the volume phase transition on the optical, hydrodynamic characteristics and size distribution of particles, respectively. The effects of the phase volume transition on the optical and hydrodynamic characteristics of particles are different. The differences are also influenced by the N,N' -methylenebisacrylamide content. With the static radius, the effects of the phase volume transition on the optical properties have been explored. In order to explore the effects of the phase volume transition on the hydrodynamic characteristics of particles and what ρ means, the accurate relationship between the optical and hydrodynamic features of particles must be understood.

Fig. 1. The experimental data and expected values of $g^{(2)}(\tau)$ for PNIPAM-1 at a temperature of 27 °C. The symbols show the experimental data and the lines show the expected values calculated under the simple assumption $R_h = 1.21R_s$.

Fig. 2. The experimental data and expected values of $g^{(2)}(\tau)$ for PNIPAM-1 at a temperature of 33 °C. The symbols show the experimental data and the lines show the expected values calculated under the simple assumption $R_h = 1.55R_s$.

Fig. 3. Values of the apparent hydrodynamic radii, mean hydrodynamic radii obtained at a scattering angle of 30° and mean static radii for PNIPAM-1 at different temperatures.

Fig. 4. Ratios obtained from the three different particle sizes measured using light scattering technique. a). The ratios $R_{h,app}^T / \langle R_s^T \rangle$ of the apparent hydrodynamic radius over the mean static radius are shown. b). The ratios $\langle R_h^T \rangle / \langle R_s^T \rangle$ of the mean hydrodynamic radius over the mean static radius are shown for PNIPAM-0, PNIPAM-1, PNIPAM-2 and PNIPAM-5 in the volume phase transition temperature range from 25 °C to 40 °C.

Fig. 5. The volume phase transition of PNIPAM-0, PNIPAM-1, PNIPAM-2 and PNIPAM-5. The phase transition is shown using the ratios of the mean static radius $\langle R_s^T \rangle$ at temperature T to that $\langle R_s^{40^\circ C} \rangle$ at 40 °C (a) and the ratios of the apparent hydrodynamic radius $R_{h,app}^T$ at temperature T to that $R_{h,app}^{40^\circ C}$ at 40 °C (b).

Fig. 6. The effects of the volume phase transition on the dimensionless parameters $\langle R_g^2 \rangle^{1/2} / \langle R_s^T \rangle$ and ρ . The results of $\langle R_g^2 \rangle^{1/2} / \langle R_s^T \rangle$ and ρ as a function of temperature T are shown in a and b, respectively.

References

- [1] Koppel, D. E. *J. Chem. Phys.* **1972**, 57, 4814-4820.
- [2] Barger, C. B. *J. Chem. Phys.* **1974**, 61, 2134-2138.
- [3] Brown, J. C.; Pusey, P. N.; Dietz, R. *J. Chem. Phys.* **1975**, 62, 1136-1144.
- [4] Berne, B. J.; Pecora, R. *Dynamic Light Scattering*; Robert E. Krieger Publishing Company: Malabar, Florida, 1990.

- [5] Zhang, X.; Wu, D.; Chu, C. *J. Polym. Sci.: Part B: Polymer Physics* **2003**, 41, 582-593.
- [6] Kratz, K.; Eimer, W. *Ber. Bunsenges. Phys. Chem.* **1998**, 102, 848-854.
- [7] Sun, Y. Unpublished.
- [8] Burchard, W. *Adv. Polym. Sci.* **1983**, 48, 1-123.
- [9] Burchard, W.; Kajiwara, K.; Nerger, D. *J. Polym. Sci.* **1982**, 20, 157-171.
- [10] Burchard, W.; Schmidt, M.; Stockmayer, W. H. *Macromolecules* **1980**, 13, 1265-1272.
- [11] Hu, T.; Wu, C. *Phys. Rev. Lett.* **1999**, 83, 4105-4107.
- [12] Wu, J.; Huang, G.; Hu, Z. *Macromolecules* **2003**, 36, 440-448.
- [13] Pusey, P. N. in *Neutrons, X-rays and Light: Scattering Methods Applied to Soft Condensed Matter*, edited by P. Lindner and Th. Zemb; Elsevier Science B.V., Amsterdam, The Netherlands, 2002.

Fig. 1.

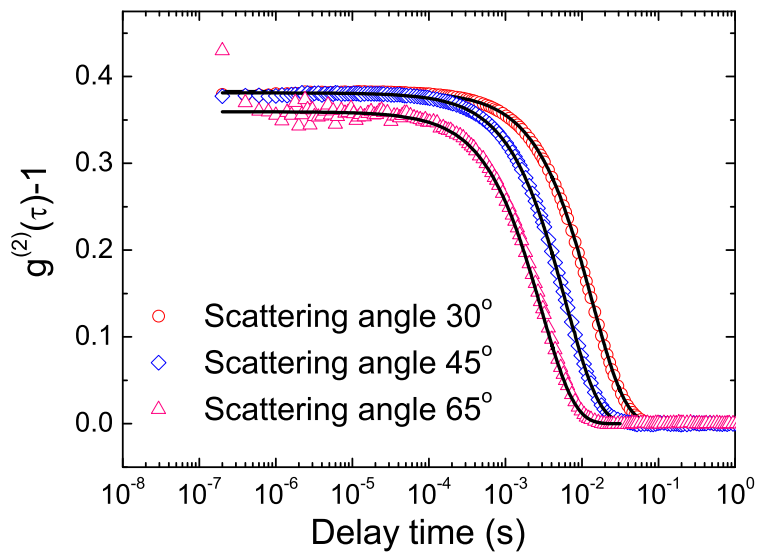


Fig. 2.

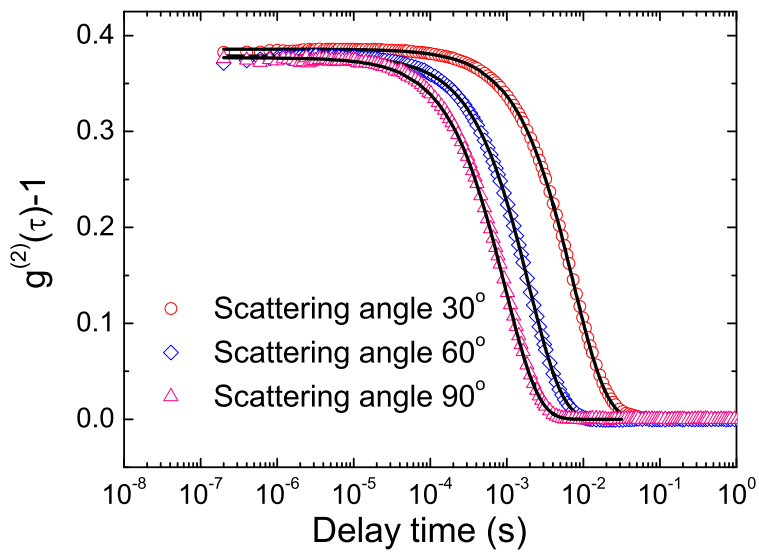
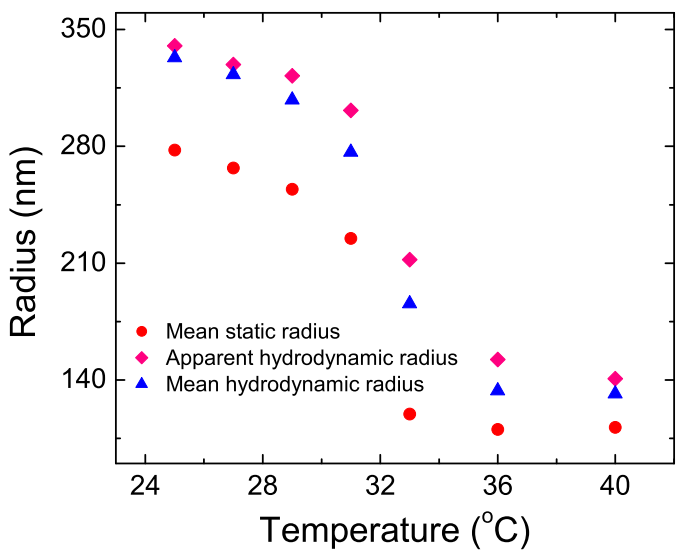
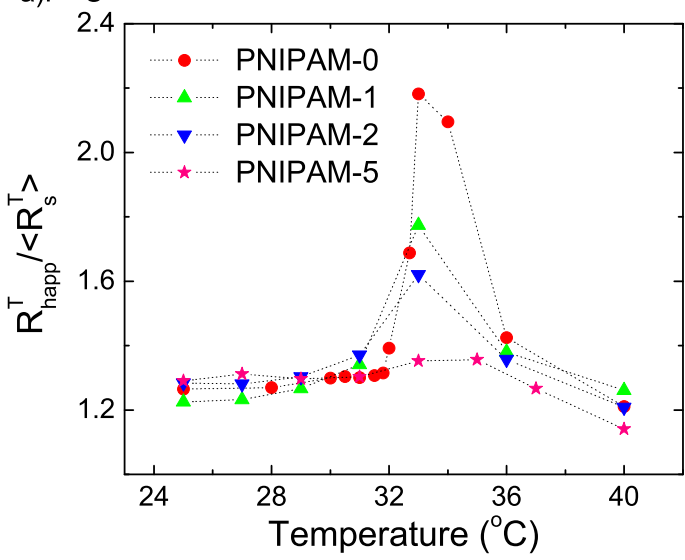


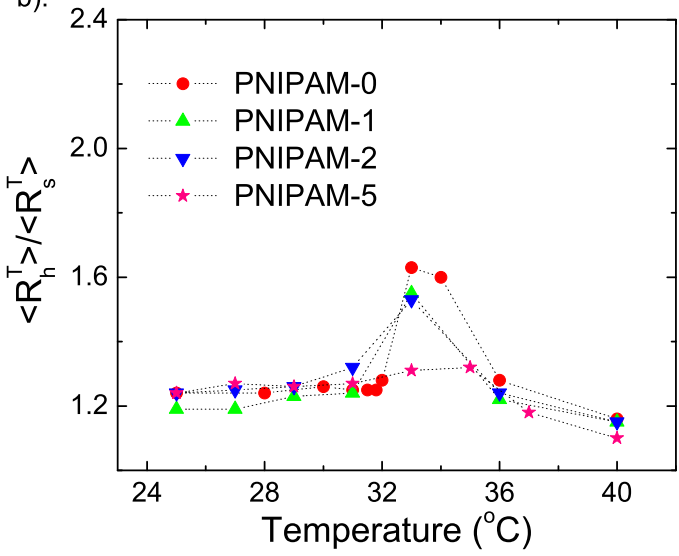
Fig. 3.



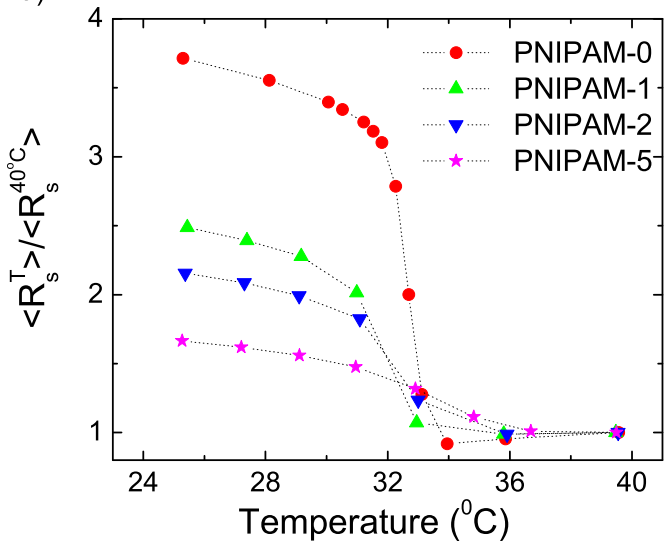
a). Fig. 4a



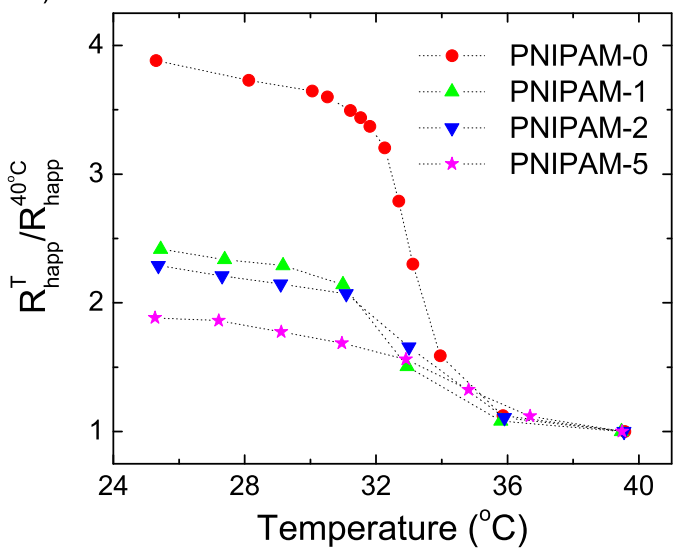
b). Fig. 4b



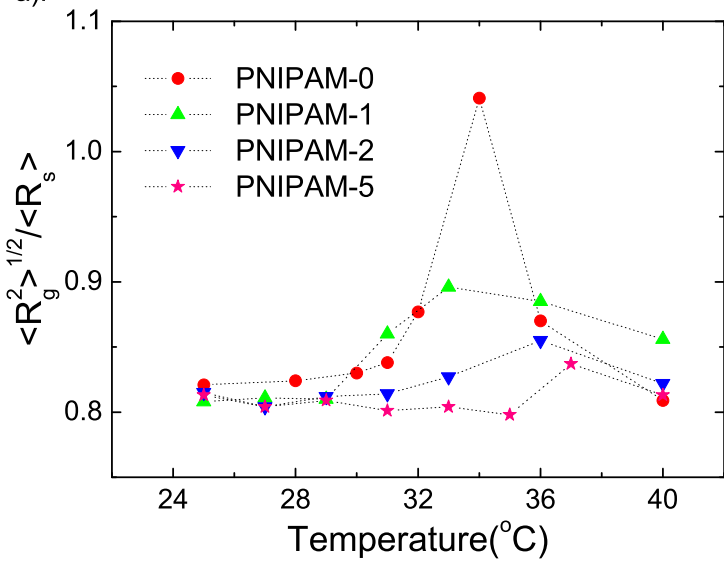
a). Fig. 5a



b). Fig. 5b



a). Fig. 6a



b). Fig. 6b

